Metallorganic Chemical Vapor Deposition and Characterization of TiO_2 Nanoparticles

Oh-Jin Jung,* Sam-Hyeok Kim, Kyung-Hoon Cheong, W. Li,† and S. Ismat Saha†

School of Environmental Engineering, Chosun University, Gwang-ju 501-759, Korea
†Department of Materials Science and Engineering, and Physical and Astronomy, University of Delaware, Newark, DE 19716, USA
Received September 7, 2002

TiO_2 nanoparticles were synthesized using the metallorganic chemical vapor deposition process. Particles with and without metal ion dopants were obtained. X-ray photoelectron and energy dispersive X-ray spectroscopic measurements confirmed the stoichiometry of the TiO_2 nanoparticles. X-ray diffraction patterns showed a polycrystalline anatase structure of TiO_2. Transmission electron microscopy revealed that these particles are of nanoscale dimensions. Exact particle size and size distribution analyses were carried out by dynamic light scattering. The average particle size was determined to be 22 nm. The nanosize particles provided large surface area for photocatalysis and a large number of free surface-charge carriers, which are crucial for the enhancement of photocatalytic activity. To improve the photocatalytic activity, metal ions, including transition metal ions (Pd^{2-}, Pt^{4+}, Fe^{3-}) and lanthanide ion (Nd^{3-}) were added to pure TiO_2 nanoparticles. The effects of dopants on photocatalytic kinetics were investigated by the degradation of 2-chlorophenol under an ultraviolet light source. The results showed that the TiO_2 nanoparticles with the metal ion dopants have higher photocatalytic activity than undoped TiO_2. The Nd^{3-} ion of these dopant metal ions showed the highest catalytic activity. The difference in the photocatalytic activity with different dopants is related to the different ionic radii of the dopants.

Key Words : TiO_2 nanoparticles, Metal ion dopants, MOCVD, Photocatalysis

Introduction

With the increase in the public awareness and concern about environmental pollutants, novel, stable, cheap, non-toxic and high catalytic activity treatment methods are in demand for the detoxification and degradation of harmful organic compounds in both aqueous and gaseous media. Besides the commonly used semiconductor oxides such as ZnO,[1,2] SnO_2,[3] and Fe_2O_3,[4] TiO_2 nanoparticles offer additional advantages in that TiO_2 is low cost, chemically inert, highly photoactive and has suitable band gap (E_g = 3.2 eV) in which its redox potential of the H_2O/·OH couple (-2.8 eV) lies. It is also self regenerating and recyclable. These properties make TiO_2 a prime candidate for broad applications, including gas sensors and photocatalysts. However, the major impediment to its widespread application, particularly indoors, resides in the fact that TiO_2 absorbs near-ultraviolet (UV) light (E_g = 3.2 eV for anatase). This band gap does not match very well with solar light. Several solutions have been proposed to increase visible light absorption in TiO_2, including doping with transition metals[5-8] and dye sensitization.[9]

In addition to the chemical modification of TiO_2 to induce visible light absorption, considerable enhancement of the absorption can also be achieved in small nanocrystals where the surface to volume ratio is large and the fraction of the surface atoms is sufficiently large. The main mechanism of light absorption in pure semiconductors is the interband electron transition. These transitions are direct because the momentum that the electron obtains from light waves is small in comparison with h/a, where "a" is the lattice constant. This absorption is especially small in direct-forbidden gap semiconductors, for which the direct electron transitions between the band centers are prohibited by the crystal symmetry. This is the case for TiO_2. However, momentum is not conserved if the absorption takes place at the boundary of the crystal, *e.g.*, at the surface or at the interface between two crystals. The possibility of indirect electron transitions there can result in the essential enhancement of light absorption. This means that considerable enhancement of the absorption can be observed in small nanocrystals, where the surface to volume ratio is very high and the share of the surface atoms is sufficiently large. The particle size at which the interface enhancement of the absorption becomes significant is around 20 nm. An additional advantage obtained in nanoparticles in the few nm size regimes is that the large surface/volume ratio makes possible the timely utilization of photogenerated carriers in interfacial processes.[10,11] The challenge is to develop a process that can produce nanoparticles of the desired size with a relatively narrow size distribution.

TiO_2 can be synthesized by several processes, including sulfate process,[12] chloride process,[12] impregnation,[5] coprecipitation,[13] sol-gel,[14-16] hydrothermal method,[8,17,18] direct oxidation of $TiCl_4$[19] and metallorganic chemical vapor deposition (MOCVD) method.[20-23] Most non-CVD processes require

*Corresponding Author: Phone: +82-62-230-6644, e-mail: ojjung@chosun.ac.kr

multiple steps to obtain monodispersed particles. In this study, MOCVD was used to prepare TiO_2 nanoparticles due to the ease and simplicity of this process. No further calcination, centrifuge or hydrothermal processing is required for crystallization or particle refinement. The control of size distribution is easily accomplished by simply controlling the temperature of the substrates and the flow rate of the precursors. Dopants can also be easily introduced into the reactor either through a solid source, separated from the Ti-precursor, or mixed in with the precursor. In the present study, the effects of transition metal and lanthanide ion doping on the photocatalytic activity of TiO_2 nanoparticles are discussed. Results of the degradation of 2-chlorophenol (2-CP) are presented. Low-level doping, particularly of Nd, resulted in a large enhancement in the photoactivity of TiO_2 nanoparticles for the photodegradation of 2-CP and pentachlorophenol.

Experimental Section

The TiO_2 nanoparticles were prepared in the metallorganic chemical vapor deposition (MOCVD) system shown in Figure 1. A horizontal stainless steel tube reactor, 5 cm in diameter and 75 cm in length was used. The central part of the reactor was externally heated by a resistive heater, and a uniform temperature of up to 1000 °C could be obtained in the 20 cm long central region. This was the region where all the sample collection was carried out. A mechanical pump was used to pump the reaction chamber down to a few mTorr base pressure. Quartz tubes, 3 cm in diameter and 12.5 cm long, and 5 cm diameter discs made of several layers of 475 mesh stainless steel screens were used in this experiment to collect the samples. Multiple layering was necessary to collect the particles efficiently. Above a critical temperature and precursor flow rate, nanocrystalline TiO_2 films were obtained on quartz tubes, which were characterized separately.[24] Before the deposition, the surfaces of the substrates were cleaned by acetone, methanol and de-ionized water. $Ti[OCH(CH_3)_2]_4$ (titanium tetraisopropoxide, TTIP, 97%) was used as the precursor for Ti. The liquid TTIP was placed in a bubbling chamber and 99.999% pure Ar was used as a carrier gas. The precursor flow rate was controlled by adjusting the temperature of the bubbling chamber and/or the flow rate of the Ar flowing through it. O_2 was added to the Ar and TTIP mixture in a baffle and the mixture was introduced into the reactor chamber for TiO_2 formation. The flow rates for O_2 and Ar were 20 and 2 sccm, respectively. Nd^{3+}, Pd^{2+}, Pt^{4+}, Fe^{3+} ion dopants were studied and the precursors used for them were neodymium (III) acetylacetonate, palladium (II) acetylacetonate, platinum (IV) acetylacetonate, and iron (III) acetylacetonate, respectively. Dopant precursors, typically in the powder form, were placed in a Cu container. The container was placed directly at a pre-determined position in the chamber. The position was determined by the temperature of the dopant, which, in turn, determined the vapor pressure of the dopant and thus the incorporation rate of the dopant in TiO_2. In this experiment the deposition temperature was 600 °C for which the positions of the dopant precursors container for Nd^{3+}, Pd^{2+}, Pt^{4+}, and Fe^{3+} were 21.5, 19, 18, and 20 cm from the center of the chamber, respectively. The doping concentration as a function of the dopant temperature was measured.

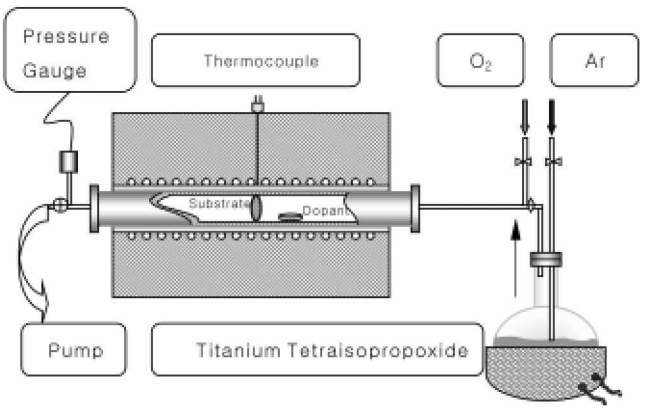

Figure 1. Schematic diagram of metallorganic chemical vapor deposition system.

Structural characterization of the doped and undoped TiO_2 samples was carried out by X-ray diffraction (XRD). θ-2θ scans were recorded using Cu K_α radiation in a Rigaku D-Max B diffractometer equipped with a graphite crystal monochromator. Precise 2θ positions and the full width at half maxima of the diffraction peaks were obtained using XFIT software.[25] Compositions of the samples were determined by X-ray photoelectron spectroscopy (XPS) and energy dispersive X-ray spectroscopy (EDS). A SSI-M Probe XPS was used employing Al K_α exciting radiation. In addition to the survey scans, high resolution scans in the Ti 2p, dopant 4d, O 1s, and C 1s regions were recorded. The Ti 2p and dopant 3d or 4d regions were used to measure the composition of the nanoparticles and to ascertain the valance states of Ti and the dopant. The measurement of average particle size and surface morphology were performed with Amray 1810T scanning electron microscopy (SEM). Transmission electron microscopy (TEM) was done in a JEOL 2000 FX TEM in order to verify the nanosize and polycrystalline structures of the particles. The size distribution of particles was investigated by Lexel 95 dynamic light scattering (DLS) apparatus, using a 488-nm laser source. To reduce the agglomeration of particles that were dispersed in methanol solvent, a 125-Watts and 50/60-Hz ultrasonic cleaner was utilized to sonicate the particle solution for about 3 minutes and a 0.45-μm filter was used to remove large agglomerations before the light scattering experiment.

Photodegradation experiments were performed in the photocatalytic reactor system. This bench-scale system consisted of a cylindrical pyrex-glass cell, 12 cm inside diameter and 30 cm length, with an inside reflective surface. A 100 watt Hg lamp was used, which was immersed in the solution with an air-cooled jacket. The maximum energy emission of UV at the wavelength of 365 nm was achieved 4 minutes after the lamp was turned on. At the cooling jacket, an energy density of 5.3 mW/cm^2 was measured and the photon

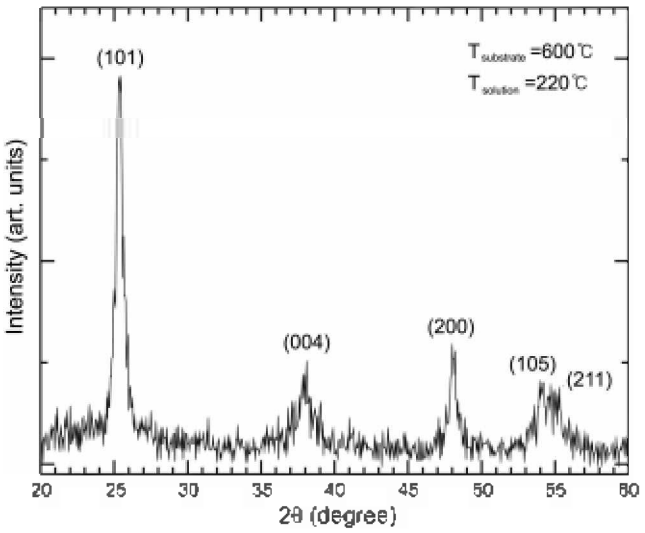

Figure 2. XRD pattern of Nd doped TiO_2 nanoparticles. All diffraction peaks belong to the anatase phase.

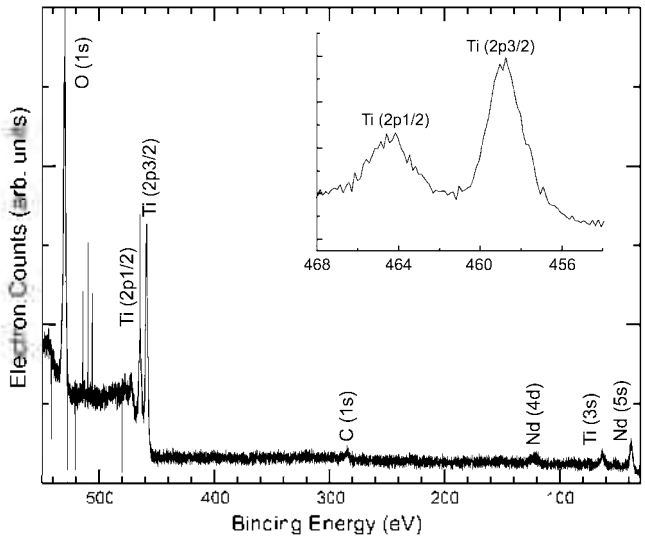

Figure 3. XPS survey and the high resolution Ti 2p region of Nd doped TiO_2 nanoparticles.

flux was calculated to be 4.42×10^{-4} Einstein/min. An aqueous solution (1000 mL) of 2-CP and the stainless steel mesh with 10 mg TiO_2 nanoparticles were placed in the photoreactor cell. A magnetic stirrer was used in the suspension and O_2 was supplied through compressed air for the oxidation reaction. During illumination, the pH value of the suspension was controlled at 9.5. After illumination, samples were collected at regular intervals in a test-tube and each sample suspension was filtered by 0.2-μm filter and then analyzed by a high performance liquid chromatograph (HPLC; Hewlett Packard series 1100 system) equipped with an UV detector (λ_{max} = 210 nm) and column [Eclipse XDB-C_{18} (50 nm × 0.5 nm)]. The eluent solvent was acetonitrile: the buffer solution was H_3PO_4/NaH_2PO_4 and pH = 3.0.

Results and Discussion

Figure 2 is a XRD pattern for TiO_2 nanoparticles doped with Nd collected on a stainless steel mesh substrate. The particles were collected at 600 °C substrate temperature and 220 °C TTIP precursor temperature. The positions of (101), (004), (200), (105) and (211) diffraction peaks confirms that the particles are polycrystalline with an anatase structure that has a tetragonal Bravais lattice. The full width at half maxima (FWHM) of the XRD peaks were measured to calculate the average particle size, using Scherrer's formula.[26] The average particle size was calculated to be approximately 27 nm. TiO_2 in anatase form is believed to be the most efficient photocatalyst during chemical reactions[27,28]. There were no other detectable peaks in the XRD pattern to suggest the presence of TiO_2 in the rutile structure. In addition, no dopant related diffraction peaks were observed. The detection limit for XRD was about 1 at.%. If the dopant forms a separate phase below this detection limit, XRD would not be able to measure it. However, TEM results also did not show any separate dopant phase. The dopants went either into the interstitial positions or substitutional sites of TiO_2 crystal structure.

The relative cation composition in the particles was determined by XPS and EDS. Figure 3 shows the XPS survey for a Nd doped sample. Only peaks associated with Ti, O, Nd and C were observed. The existence of a very small C peak is possibly due to surface contamination. Nd concentration was measured to be about 1 at.%. This concentration was also confirmed by EDS (data not shown), which suggest a uniform distribution of Nd in the nanoparticles. The insert in Figure 3 is the magnified Ti 2p region showing two peaks located at 458.4 eV and 464.1 eV, respectively. The peaks for metallic Ti^0 were expected at 453.8 ($2p_{3/2}$) and 459 ($2p_{1/2}$) eV.[29] The shifts in Ti ($2p_{3/2}$) and Ti ($2p_{1/2}$) peak positions are due to the presence of tetravalent Ti^{4+}, as expected in TiO_2. The change in the separation between the Ti ($2p_{3/2}$) and Ti ($2p_{1/2}$) peaks is also consistent with the formation of TiO_2.[29,30] Nd 4d peak occurs

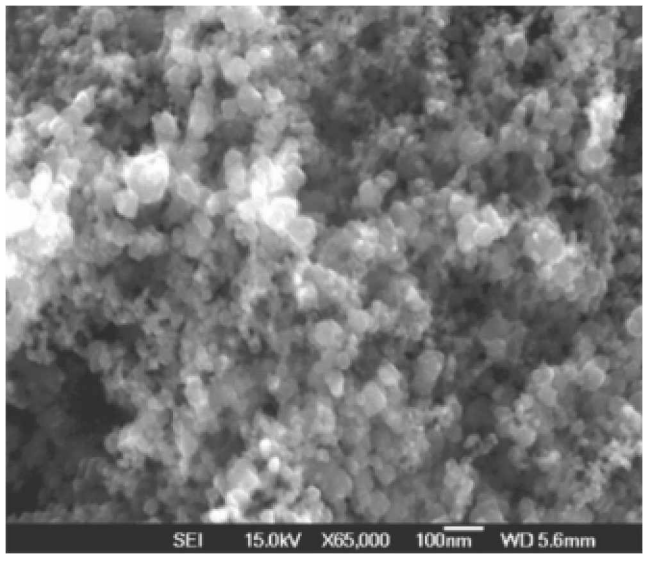

Figure 4. SEM image of TiO_2 nanoparticles grown at 600 °C.

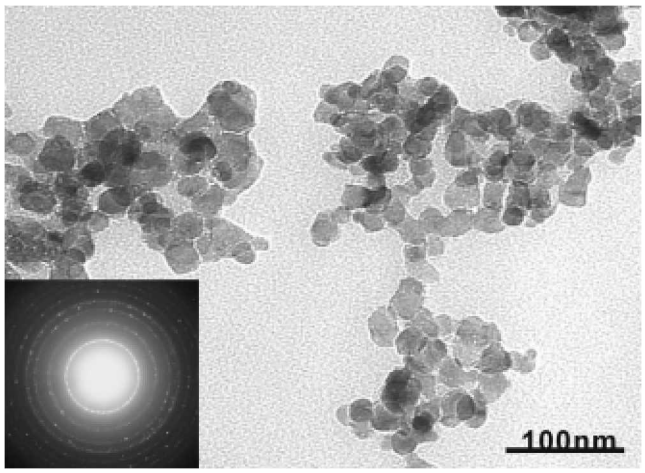

Figure 5. TEM bright field image of polycrystalline TiO_2 nanoparticles and selected area diffraction pattern. TiO_2 nanoparticles were deposited at 600 °C.

at 122 eV, which is shifted from the Nd^0 peak position (118 eV)[29] suggesting that Nd is present as Nd^{3+}.[31]

The surface morphology of the sample was examined by scanning electronic microscopy (SEM). Figure 4 is a SEM picture of the Nd doped TiO_2 nanoparticles. The aggregated nanostructured TiO_2 particles are visible. The micrograph confirms the nanometer size of the TiO_2 particles. Although SEM micrographs can give a rough measure of the particle size, TEM was used for more accurate particle size measurement. Figure 5 shows a TEM bright field image with the diffraction pattern as an insert. The average particle size measured was about 22 nm, consistent with the grain size measured by XRD. The electron diffraction pattern corresponds to that of TiO_2. Figure 6 shows the DLS results, indicating that the TiO_2 nanoparticles were distributed in the range of 20-25 nm with a short tail towards the larger particle size. The larger particles could not be eliminated even after extended sonication.

The photodegradation experiments were carried out on

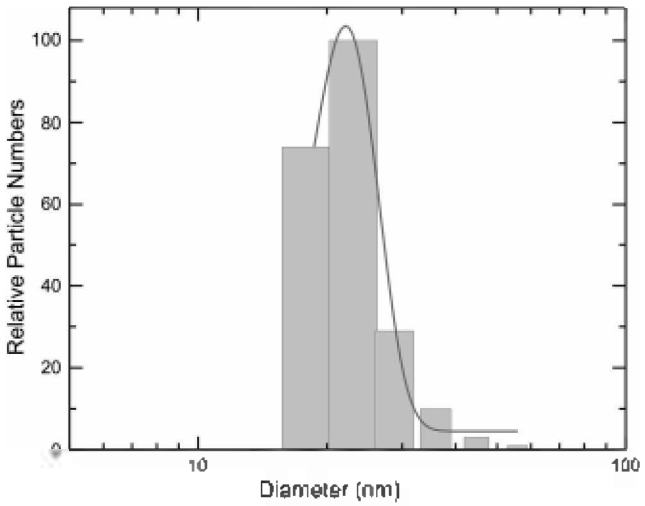

Figure 6. Particle size distribution of TiO_2 nanoparticles obtained by dynamic light scattering.

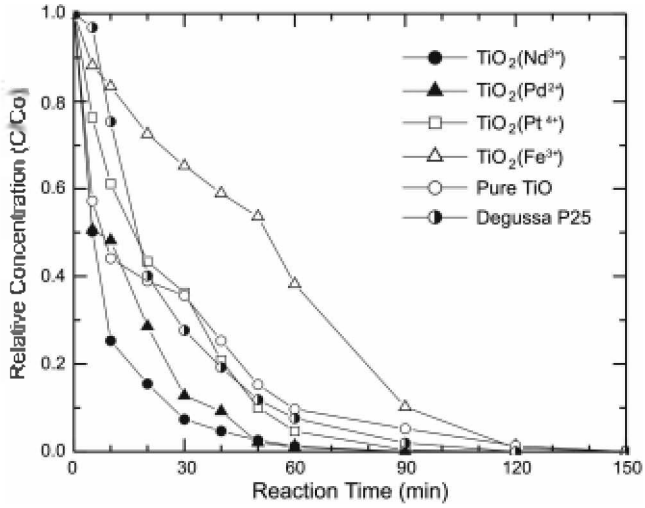

Figure 7. Photodegradation of 2-chlorophenol with Degussa P25, undoped TiO_2 and different metal ion (Nd^{3+}, Pd^{2+}, Pt^{4+}, Fe^{3+}) doped TiO_2 under a UV light source. Initial concentration of 2-CP C_0 = 50 mg and volume = 1000 mL with pH 9.5.

samples doped with transition metal Pd, Pt, Fe and lanthanide Nd. The doping level in all four cases was kept constant at about 1 at.%. The activities for the photodegradation for 2-CP are compared in Figure 7. The figure also shows the photoactivities of the undoped TiO_2 nanoparticles and Degussa P25 standard. The results show that the activities for the photodegradation of 2-CP have been enhanced in most cases. In particular, for Nd doped TiO_2, the time for 90% destruction of 2-CP has been reduced to 25 minutes from 60 minutes in the case of undoped TiO_2 and Degussa P25. The apparent quantum yield can be calculated, which is the ratio of the number of pollutant molecules destroyed to the number of photons absorbed. Assuming that the fraction of the absorbed photons by TiO_2 is 1, the apparent quantum yields were calculated for doped and undoped TiO_2, and are shown in Table 1. The quantum yield of 2-CP suspension with Nd doped TiO_2 catalyst is almost 3 times that of pure TiO_2 and 2.5 times that of Degussa P25. However, the Fe doped TiO_2 had the lowest yield, which is only 0.4 times that of pure TiO_2. The lack of enhancement of photocatalytic activity by Fe doping is not surprising. There have been previous studies that show similar results for Fe on the

Table 1. Estimations of initial photodegradation rate, UV photon flux, and apparent quantum yield for aqueous solutions of 2-CP with doped and undoped TiO_2 nanoparticles in the reactor

Catalyst	Initial rate $10^6 R^{in}$ (mol/min)	Photon flux $10^4 R_{o(365)}$ (Einstein/min)	Quantum yield $-10^2 \Phi_{2CP} = R^{in}/R_{o(365)}$
TiO_2 (Nd^{3+})	29.2 ± 0.25	4.42	6.61 ± 0.06
TiO_2 (Pd^{3+})	17.6 ± 0.82	4.42	3.98 ± 0.19
TiO_2 (Pt^{4+})	12.9 ± 0.47	4.42	2.92 ± 0.11
TiO_2 (Fe^{3+})	3.74 ± 0.64	4.42	0.84 ± 0.14
Pure TiO_2	9.72 ± 0.82	4.42	2.20 ± 0.19
Degussa P25	11.7 ± 0.25	4.42	2.65 ± 0.06

photodegradation of the vinyl chloride.[13] The reason for the lack of photocatalytic activity enhancement by Fe is not completely understood but could be related to non-optimal valency of Fe, the ionic radii of Fe and the attachment of phenol to Fe. The accurate determination of Fe oxidation state when it is present in such low concentrations is difficult due to the problem of satisfactorily resolving the Fe 3p region of the XPS spectrum. Currently, experiments are being designed to increase the concentration of the dopants, which will make it easier to determine the Fe oxidation state.

The primary driving force in this research is to study the photocatalytic characteristics of TiO_2 nanoparticles and the effect of metal ion doping on its performance. In photocatalysis, the number of free charges on the surface determines the efficiency of the catalyst. For large particles, the volume recombination of electrons and holes dominates. This largely reduces the numbers of free charges on the surface, deteriorating the photocatalytic activity. The recombination of hole (h^+)-electron (e^-) pairs are suppressed because the nanosize particles of TiO_2 have many defect sites where photoexited electrons can be trapped. Also, photoreactivity increases with a decrease in the surface area of the nanoparticles, thereby increasing the efficiency of photocatalyst. For optimum efficiency, there is a critical size below which the surface recombination of electrons and holes becomes dominant due to the increased surface to volume ratio.[15,32] The activity of TiO_2 is also dopants dependent. Different dopants have different effects on impeding the transportation of electrons and holes from the interface to the surface. Consequently, different dopants can have different effects on catalyst efficiency.

As discussed earlier, XRD results confirmed the presence of only the anatase phase in the TiO_2 nanoparticles and that no separate dopant related phase is present in the particles. This suggests that the dopant (Fe, Pt, Pd, Nd) either goes to the substitution sites on TiO_2 lattice or to the octahedral interstitial sites. For chlorophenol degradation, an oxidation reaction, the trapping of electrons is critical. In nanoparticles, electron trapping reduces surface recombination and allows holes to diffuse to the particle surface and participate in the oxidation reaction. Any dopant that effectively increases the localized positive charge will improve the oxidation of chlorophenols. The effective sizes of ions are shown in Table 2.[33,34] Nd^{3+} has the largest ionic radii, 0.983 Å, much larger than that of Ti^{4+}, 0.605 Å. Pd^{2+} has ionic radii, which is also relatively larger than that of Ti^{4+}. Fe^{3+} and Pt^{4+}, on the other hand, have ionic radii that are relatively small and comparable to that of Ti^{4+}. The similarity of ionic radii promotes substitutional incorporation of the dopants. The substitutionally incorporated dopant is less useful in the charge trapping since the local charge distribution is only slightly disturbed, if at all. On the other hand, Nd^{3+} and Pd^{2+} ions are much larger than Ti^{4+}. Therefore, it is energetically favorable for them to preferentially go into the larger octahedral interstitial sites in the anatase lattice.[35] The high oxygen affinities of Nd and Pd cause a strong dopant-oxygen bond. This effectively creates a localized positive charge around Ti and/or forms an oxygen vacancy. Both of these possibilities help form electron traps, increasing the lifetime of holes.

Table 2. Ionic radii for a coordination number of 6

Ions	Fe^{3+}	Pd^{2+}	Pt^{4+}	Nd^{3+}	Ti^{4+}
Ionic radii (Å)	0.645	0.86	0.625	0.983	0.605

Under the condition of efficient electron trappings, the interfacial transferring becomes easier for the holes, which finally react with water and oxygen to form more active hydroxyl radicals. It is the hydroxyl radicals that participate in the oxidation reaction of 2-CP. In our experiment, the pH value was kept constant and also there was excessive O_2 supplied. Thus, the generation rate of hydroxyl radicals diffused into the aqueous solution is basically determined by the number of holes transferred to the surface of TiO_2 solid phase. The holes, with larger quantity or longer lifetime, have a tendency to produce more radicals until a steady state, with a balance of the radical consumption and production, is reached. According to this pseudo-first-order degradation process, the destruction rate of 2-CP aqueous solution can be addressed as:

$$-\frac{d[C]}{dt} = K_{opp}[OH^*][C] \quad (1)$$

where, $[OH^*]$ is the hydroxyl radicals concentration, $[C]$ is 2-CP concentration, t is reaction time, and K_{app} is apparent reaction rate which can be affected by the power of lamp, concentration of catalyst, etc..[36] Apparently, with the same reactor geometry, power of UV lamp, and initial concentration of 2-CP and TiO_2, the degradation rate or number of radicals is closely related to the dopant type. The chemical reaction and the ionic radii effects discussed above suggest that Fe does not help the 2-CP oxidation process at all and Pt helps only slightly. Pd and Nd can enhance the efficiency, especially Nd^{3+}, having large ionic radii that causes the localized charging effect.[37]

Conclusions

We have synthesized doped and undoped TiO_2 nanoparticles by MOCVD on a variety of substrates. Within a certain range of the growth temperatures the TiO_2 nanoparticles were crystalline and had anatase structure. The particles were doped with a variety of transition metals and lanthanide ion dopants. The effect of the dopants (~1%) on the photocatalytic activity for the destruction of 2-CP was measured. Nd doping was most effective in the enhancement of the photoactivity of the TiO_2 nanoparticles. The 90% destruction time of 2-CP was reduced from 60 minutes for the undoped TiO_2 nanoparticles to 25 minutes for the 1 at.% Nd doped nano TiO_2. The apparent quantum yield was 2.5 times that of Degussa P25 and 3 times that of undoped TiO_2. The enhancement of the photocatalytic efficiency was related to the size differences between the host Ti^{4+} ionic radii and the dopant's ionic radii. Smaller ionic radii Fe^{3+} did not help the oxidation of 2-CP whereas all the larger ionic radii dopants

did, particularly Nd^{3+}. Fe, presumably, goes on the substitutional sites while Pd and Nd go on the interstitial sites. Further experiments, including near edge X-ray absorption fine structure (NEXAFS) and XPS, are being carried out to ascertain the position of the dopants in the TiO_2 lattice.

Acknowledgment. This study was supported by research funds and facilities from Chosun University, Korea and University of Delaware, USA, 2001.

References

1. Hotchandani, S.; Kamat, P. V. *J. Electrochem. Soc.* **1992**, *139*, 1630.
2. Rensmo, H.; Keis, K.; Lindström, H.; Söedergren, S.; Solbrand, A.; Hagfeldt, A.; Lindquist, S.-E.; Wang, L. N.; Muhammed, M. *J. Phys. Chem.* **1997**, *B 101*, 2598.
3. Bedja, I.; Kamat, P. V. *J. Phys. Chem.* **1995**, *99*, 9182.
4. Bjorksten, U.; Moser, J.; Gratzel, M. *Chem. Mater.* **1994**, *6*, 858.
5. Litter, M. I.; Navio, J. A. *J. Photochem. Photobiol. A: Chem.* **1994**, *84*, 183.
6. Bickley, R. I.; Gonzalez-Carreno, T.; Gonzalez-Elipe, A. R.; Munuera, G.; Palmisano, L. *J. Chem. Soc. Faraday Trans.* **1994**, *90*, 2257.
7. Murata, Y.; Fukuta, S.; Ishikawa, S.; Yokoyama, S. *Sol. Energy Mater. Sol. Cells* **2000**, *62*, 157.
8. Wang, Y.; Cheng, H.; Hao, Y.; Ma, J.; Li, W.; Cai, S. *J. Mater. Sci.* **1999**, *34*, 3721.
9. Bach, U.; Lupo, D.; Comte, P.; Moser, J. E.; Weissortel, F.; Salbeck, J.; Spreitzer, H.; Gratzel, M. *Nature* **1998**, *395*, 583.
10. Nozik, A. J.; Memming, R. *J. Phys. Chem.* **1996**, *100*, 13061.
11. Grela, M. A.; Brusa, M. A.; Colussi, A. J. *J. Phys. Chem.* **1997**, *B 101*, 10986.
12. *Kirk-Othmer Encyclopedia of Chemical Technology*; Howe-Grant, M., Ed.; John Wiley & Sons, Inc.; 1997; Vol. 24, p 225.
13. Palmisano, L.; Augugliaro, V.; Sclafani, A.; Schiavello, M. *J. Phys. Chem.* **1988**, *92*, 6710.
14. Choi, W.; Termin, A.; Hoffermann, M. R. *J. Phys. Chem.* **1994**, *98*, 13669.
15. Zhang, Z.; Wang, C.-C.; Zakaria, R.; Ying, J. Y. *J. Phys. Chem.* **1998**, *B 102*, 10871.
16. Wang, C.-C.; Zhang, Z.; Ying, J. Y. *Nano Structured Mater.* **1997**, *9*, 583.
17. Cheng, H.; Ma, J.; Zhao, Z.; Qi, L. *Chem. Mater.* **1995**, *7*, 663.
18. Wang, Y.; Hao, Y.; Cheng, H.; Ma, J.; Xu, B.; Li, W.; Cai, S. *J. Mater. Sci.* **1999**, *34*, 2773.
19. Akhtar, M. K.; Xiong, Y.; Pratsinis, S. E. *AIChE J.* **1991**, *37*, 1561.
20. Ding, Z.; Hu, X.; Lu, G. Q.; Yue, P.-L.; Greenfield, P. F. *Langmuir* **2000**, *16*, 6216.
21. Okuyama, K.; Kousaka, Y.; Tohge, N.; Yamamoto, S.; Wu, J. J.; Flagan, R. C.; Seinfeld, J. H. *AIChE J.* **1986**, *32*, 2010.
22. Okuyama, K.; Jeung, J.-T.; Kousaka, Y. *Chem. Eng. Sci.* **1989**, *44*, 1369.
23. Okuyama, K.; Ushio, R.; Kousaka, Y.; Flagan, R. C.; Seinfeld, J. H. *AIChE J.* **1990**, *36*, 409.
24. Ismat Shah, S.; Li, W. unpublished.
25. Freeware form http://www.ccp14.ac.uk/tutorial/xfit-95/.
26. Cullity, B. D. *Elements of X-Ray Diffraction*; Addison-Wesley: Menlo Park, CA, 1978.
27. Sclafani, A.; Palmisano, L.; Davi, E. *J. Photochem. Photobiol. A: Chem.* **1991**, *56*, 113.
28. Vidal, A.; Herrero, J.; Romero, M.; Sanchez, B.; Sanchez, M. *J. Photochem. Photobiol. A: Chem.* **1994**, *79*, 213.
29. *Handbook of X-ray Photoelectron Spectroscopy*; Wagner, C. D.; Riggs, W. M.; Davis, L. E.; Moulder, J. F.; Muilenberg, G. E., Eds.; Perkin-Elmer corporation: 1979.
30. Sen, S. K.; Riga, J.; Verbist, J. *Chem. Phys. Lett.* **1976**, *39*, 560.
31. Sarma, D. D.; Rao, C. N. R. *J. Electron Spectrosc. Relate. Phenom.* **1980**, *20*, 25.
32. Beydoun, D.; Amal, R.; Low, G.; McEvoy, S. *J. Nanoparticle Res.* **1999**, *1*, 439.
33. Shannon, R. D. *Acta Crystallogr.* **1976**, *A 32*, 751.
34. Shannon, R. D.; Prewitt, C. T. *Acta Crystallogr.* **1969**, *B 25*, 925.
35. Jung, O. J.; Kim, I. K.; Saha, I. S. (Structure and size distribution of Nd(III) doped TiO_2 nanoparticle) *Material Science and Engineering B*, in press.
36. Fotou, G. P.; Pratsinis, S. E. *Chem. Eng. Comm.* **1996**, *151*, 251.
37. Jung, O. J. *Bull. Korean Chem. Soc.* **2001**, *22*, 1188.